Experimental investigation of dust explosions with a focus on black mass in battery recycling

Journal of Loss Prevention in the Process Industries 94 (2025) 105526

Contents lists available at ScienceDirect

Journal of Loss Prevention in the Process Industries

journal homepage: www.elsevier.com/locate/jlp

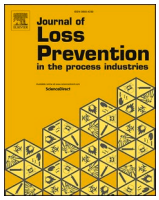

Experimental investigation of dust explosions with a focus on black mass in battery recycling

Chen Huang [a,*], Andrei N. Lipatnikov [b], Cecilia Lövström [a], Nijaz Smajovic [c], Leena Andersson [c], Abdelrahman Ismail [c]

[a] Division of Safety and Transport, RISE Research Institutes of Sweden, Sven Hultins Plats 5, SE-412 58, Gothenburg, Sweden
[b] Chalmers University of Technology, Department of Mechanics and Maritime Sciences, SE-412 96, Gothenburg, Sweden
[c] Division of Material and Production, RISE Research Institutes of Sweden, Brinellgatan 4, SE-504 62, Borås, Sweden

ARTICLE INFO

Keywords:
Dust explosion
Lithium-ion battery
Recycling
Black mass
Particle size distribution
Water content
Organic solvent
Process safety

ABSTRACT

The number of batteries in various applications at end-of-life and production waste from battery gigafactories increase significantly. At the same time, new EU regulations are introduced to promote battery recycling, which is a new and rapidly growing business. Large amounts of combustible dust are generated in battery recycling. Managing combustible dust hazards at the battery recycling plants is one of the key factors to minimize the incidents and down time and, therefore, to improve the work environment, and to increase the profitability of the business. Accordingly, the present work aims at exploring the risk of explosion of black mass dusts associated with battery recycling. Specifically, four black mass samples from different battery recycling plants are experimentally investigated. Microscope images, particle size distribution, water content and organic carbonates are analyzed. Dust explosion experiments are performed in a 20-L vessel. Parameters including dust concentration, ignition energy, ignition delay, dust injection pressure are varied. Results show that a 10 kJ ignition energy cannot generate high explosion overpressure, whereas an ignition energy of 20 kJ yields an explosion overpressure above 6 bar for black mass sample C at a concentration of 300 g/m^3. The obtained experimental results are compared with published data on various explosion-related characteristics of other dusts relevant to battery recycling, in particular, aluminum and graphite dusts.

1. Introduction

The strong momentum in electrification of transport sector, especially the rise of electric vehicles (EVs) and associated battery gigafactories, are pushing forward development of a closed-loop battery recycling value chain. Moreover, batteries have become increasingly crucial for daily electricity storage, maintaining balance within electricity grids, and strengthening renewable energy sources from wind and solar power. The next generation of batteries is extremely challenging to manufacture due to stringent specifications for high capacity, high power, long lifecycle, and safety. As a result, significant amounts of production waste are generated, especially during the ramp-up in newly established gigafactories. Approximately 70 GWh or 400 kilotons of annual production waste is expected to need recycling in Europe by 2025 (Navarro et al., 2022).

At the same time, (i) intensified EU regulations (Directive 2000/53/EC, 2000, Directive 2012/19/EU, 2012, Regulation (EU) 2023/1542, 2023), (ii) a strong desire to localize supply chains and safeguard critical raw materials, i.e., lithium, cobalt, manganese, nickel, natural graphite, copper, aluminium, etc. (CRM list, 2023, Regulation (EU) 2024/1252, 2024), and (iii) environmental issues associated with the mining of these materials (Harper et al., 2019), are driving the forward the battery recycling industry in Europe.

The widely used recycling technique in Sweden consists of preprocessing or pretreatment of batteries, including sorting, stabilization, dismantling, separation, and recycling (Ali et al., 2022). In the preprocessing or mechanical recycling process, there are many steps that involve handling of combustible dust; see Fig. 1. For instance, the dismantling process involves mechanically dismantling the battery packs by ripping, shredding, crushing, and milling into a black material of varying sizes and shapes. Further on, materials such as plastic, steel, iron, aluminium, and copper, are separated from the black material by various techniques such as sieving, magnetic, electrostatic, eddy current and gravity density separations (Ali et al., 2022). A final product, black

* Corresponding author.
E-mail address: chen.huang@ri.se (C. Huang).

https://doi.org/10.1016/j.jlp.2024.105526
Received 6 August 2024; Received in revised form 14 November 2024; Accepted 2 December 2024
Available online 8 December 2024

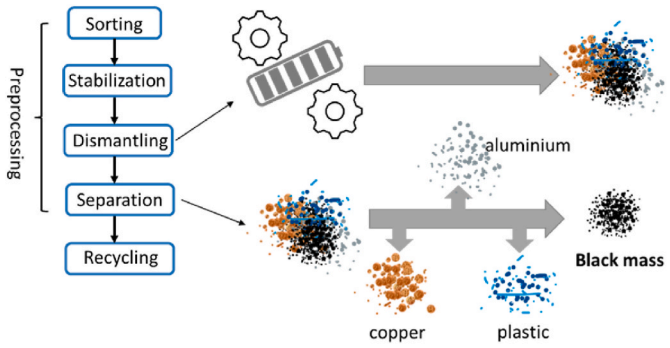

Fig. 1. Overview of the battery recycling process, adapted from Ali et al. (2022).

mass, enriched in precious metals and graphite, and a granular material made up of the shredded cathodes and anodes of the batteries, is obtained for further hydro- or pyrometallurgical extractions. The composition of black mass varies widely due to differences in feed material and shredding processes.

Safe and effective operation at battery recycling plants is crucial to meet the climate goals. Incidents statistics collected by Yuan et al. (2015) shows that dust explosion incidents are in close relationship with industrial activities. As the battery recycling capacity is expected to grow exponentially in the coming years, managing combustible dust hazards at the battery recycling plants will be one of the key factors to minimize the incidents and down time and, therefore, to improve the work environment and to increase the profitability of the business.

For instance, an explosion occurred at an old battery recycling plant of Contemporary Amperex Technology Corporation (CATL) with a capacity of 15 000 ton/year for battery ternary precursors on January 7th, 2021 in Hunan Province, China. It was unclear if the explosion was directly related to combustible dust. However, according to the recycling firm, the explosion was caused by waste aluminium foil caught fire in a garbage dump (Argus, 2021). The blast generated a mushroom cloud in the sky that could be seen from several kilometres away. The incident led to one fatality and 20 injuries (Independent, 2021). Another fatal incident occurred at a battery factory in northern Sweden on November 4th, 2023, where a 25-year-old man suffered serious injury during an explosion (SVT Nyheter, 2023a, 2023b). The explosion occurred during a maintenance of a cleaning equipment. The injured person was reported passed away on December 15th, 2023. The investigation showed that the explosion was related to aluminium dust

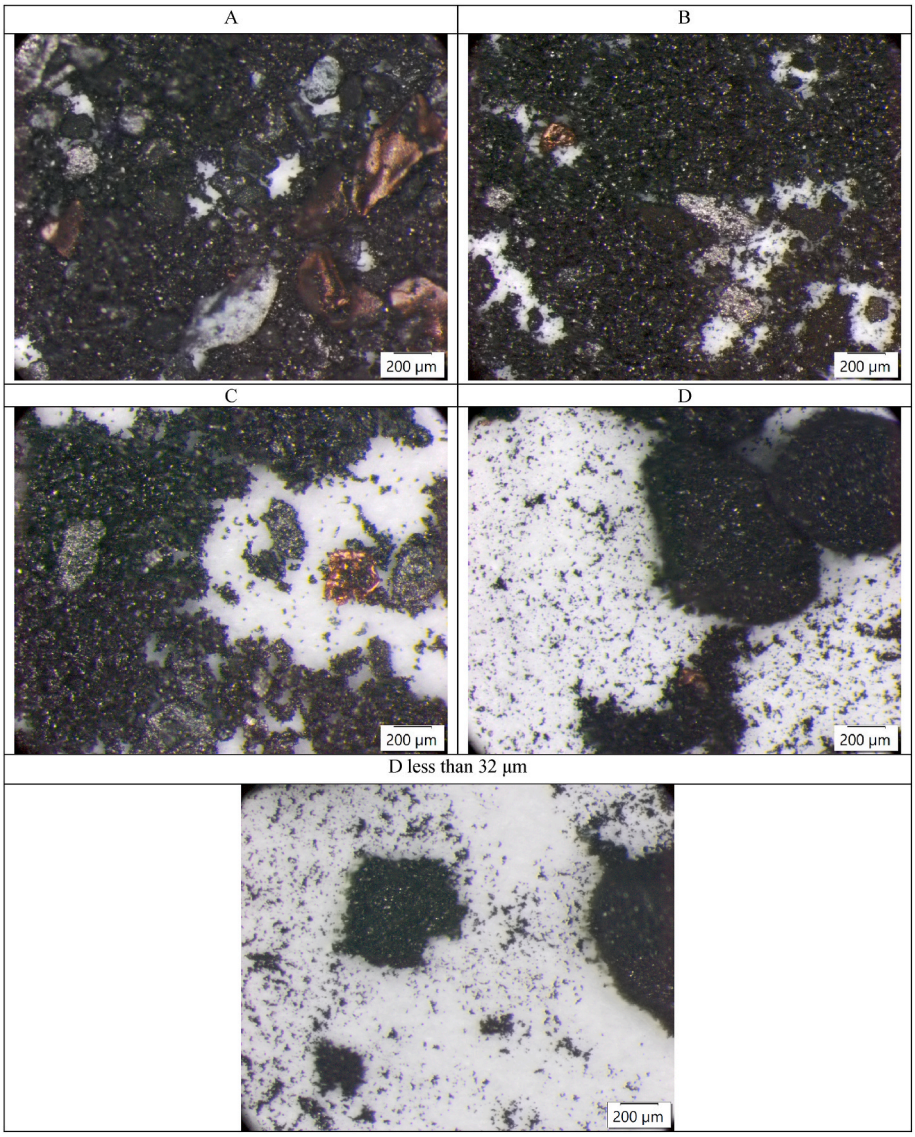

Fig. 2. Microscope images of samples A, B, C, D, and D sieved below a particle size of 32 µm.

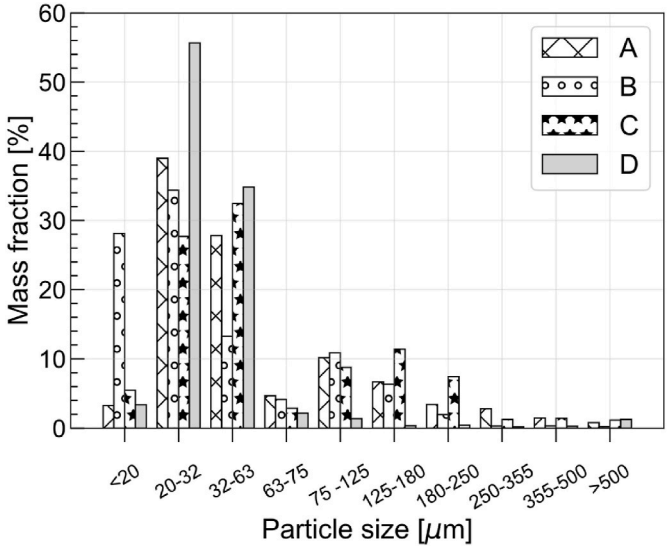

Fig. 3. Comparison of particle size distributions of four black mass samples.

Table 1
Characteristics of particle size distributions and water contents.

Parameters	Sample A	Sample B	Sample C	Sample D
D_{10} [μm]	12.76	3.55	12.62	11.90
D_{50} [μm]	32.00	20.18	37.16	23.40
D_{90} [μm]	140.40	97.67	163.66	45.11
σ_d [-]	3.99	4.66	4.06	1.42
D_{32} [μm]	37.68	21.57	39.32	30.61
water content [-]	0.70%	0.36%	0.19%	0.36%

Table 2
The content (weight) of Semi Volatile Organic Compounds (SVOC) in black mass determined by GCMS method.

Chemical	Sample A	Sample B	Sample C	Sample D
Ethylene carbonate [-]	2.99 %	0.014 %	–	3.00 %
Ethane-1,2-diyl diisobutyl decarbonate [-]	0.07 %	–	–	–
Ethylene glycol [-]	–	0.14 %	–	–
Propylene glycol [-]	–	0.08 %	–	–
N-Methyl-2-pyrrolidone [-]	–	0.07 %	–	–
Triphenyl phosphate [-]	–	–	–	0.12 %
4-(tert-Butyl)phenyl diphenyl phosphate [-]	–	–	–	0.12 %

(Elektrikern, 2024).

Several articles highlighted the dust explosion risks during battery recycling, e.g., for graphite dust (Kim et al., 2021; Yi et al., 2021; Yu et al., 2021). Furthermore, a report (Sattar et al., 2022) highlights a risk of black mass hazards. For instance, due to incomplete discharge of the batteries, the elemental lithium at the anode (LiC_6) may react with water (moist in the air) and release hydrogen and heat, i.e., $2Li + 2H_2O \rightarrow 2LiOH + H_2$. Subsequently the released hydrogen may ignite organic carbonates, e.g., ethyl methyl carbonate ($C_4H_8O_3$), or black mass, resulting in major secondary explosions. However, there is limited test data for dust explosion characteristics of black mass and production scrap due to potential health risks in testing such dusts and this knowledge gap should be bridged.

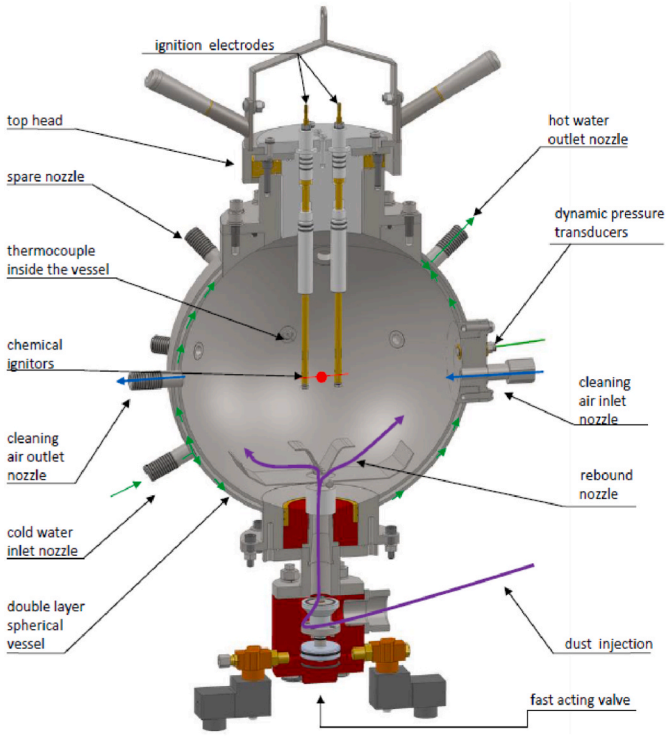

Fig. 4. 20-litre spherical vessel (Anko, 2017).

Table 3
Summary of parameters and their variation range.

Parameters	Variation range
Material	A, B, C, D
Dust concentration [g/m^3]	100, 125, 200, 300 400, 500, 600, 750, 1500, 2500
Ignition energy [kJ]	2, 10, 20, 30
Ignition delay [ms]	50, 60, 70 80
Injection pressure [bar (g)]	19.6, 20, 20.4

Accordingly, the present paper (i) reports material properties of battery recycling material, in particular, four types of black mass associated with Nickel-Cobalt-Manganese (NCM) battery chemistry, (ii) summarizes dust explosion experiments with the black mass, and (iii) compares the dust explosion parameters of black mass measured in this study with those of graphite and aluminium dusts reported in the literature.

2. Black mass samples

Four types of black mass material were provided by two battery recycling firms. These samples were obtained in mechanical processes using batteries associated with NCM chemistry. In the following, the samples are named A, B, C, and D. The first three samples were provided by one battery recycling factory and sample D was given by another battery recycling facility. Before explosion tests, certain material properties were measured, as reported in the next subsections.

2.1. Microscope images

Black mass was investigated using a stereo microscope from Olympus SZX 16. The obtained microscope images show that samples A, B and C

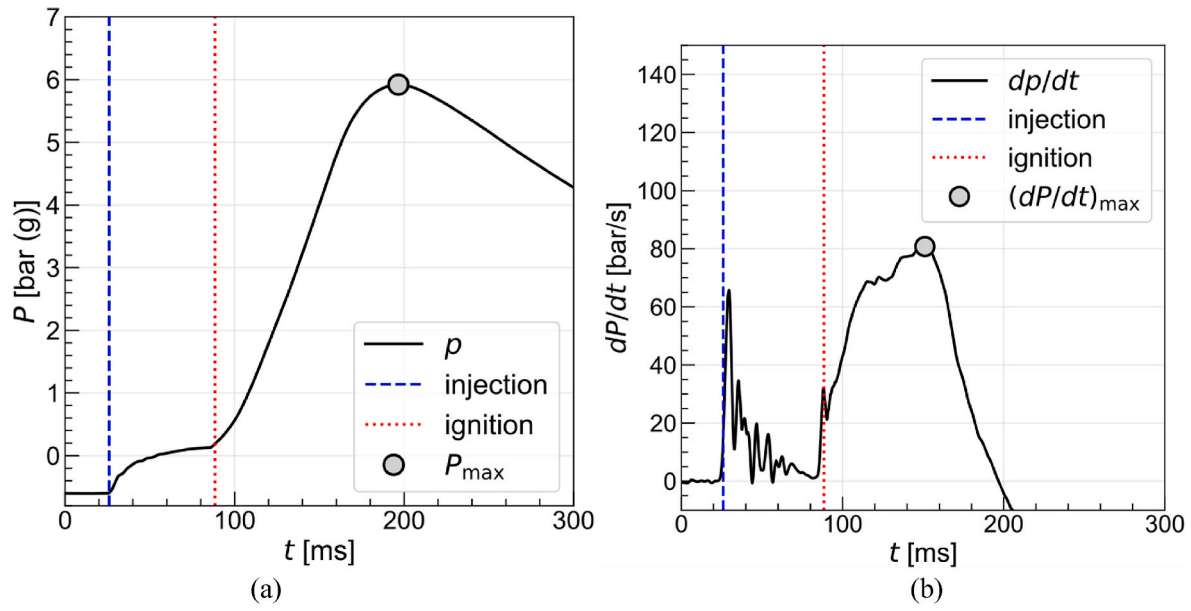

Fig. 5. Explosion overpressure (a) and pressure rise rate (b) versus time for black mass sample C. Dust concentration is equal to 300 g/m^3. Ignition energy is equal to 20 kJ. Dust injection timing and the ignition delay are marked in blue dashed line and red dotted line, respectively. (For interpretation of the references to colour in this figure legend, the reader is referred to the Web version of this article.)

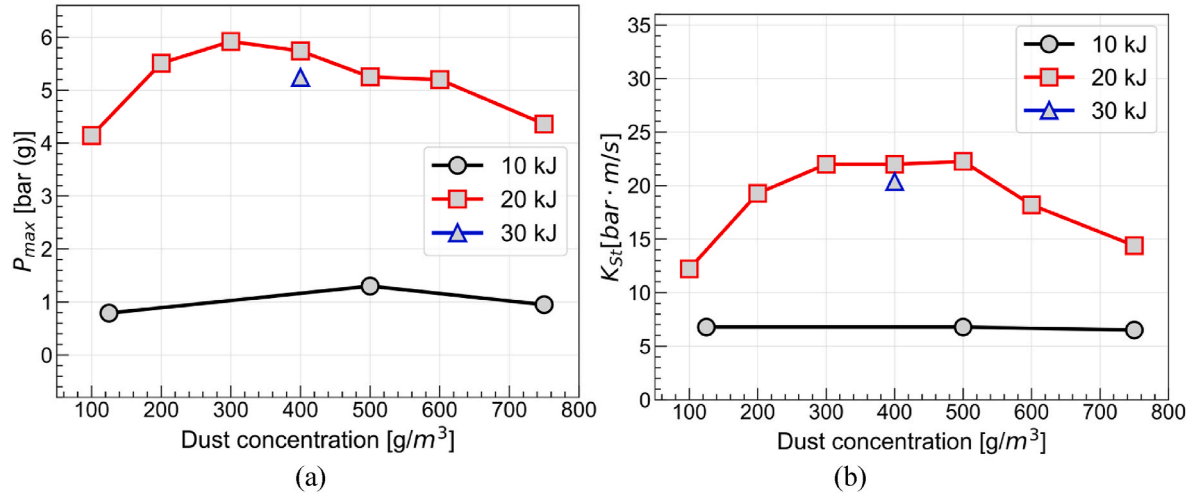

Fig. 6. Maximum explosion overpressure (a) and deflagration index (b) versus concentration of black mass sample C at different ignition energies.

from one battery recycling plant contain larger pieces of particles, probably copper and aluminium foil, when compared to sample D; see Fig. 2. Moreover, sample D shows obvious agglomeration, which is not very well observed for samples A, B and C.

2.2. Particle size distribution and water content

Particle size distributions were measured using a sieve shaker manufactured by Retsch of series AS200 control, equipped with sieve mesh sizes of 20, 32, 63, 75, 125, 180, 250, 350, 500, 600, 710, 800, 1000 μm and a sieve frame diameter of 200 mm. The sieves were arranged in a stack, with the coarsest sieve at the top and finest sieve at the bottom. The top sieve was filled with approximately one third of the volume with the powder material. When shaking the material in a 3-dimensional direction, particles larger than a sieve mesh size remained on the sieve.

The material weights on the sieves were then measured, and a particle size distribution was determined. The sieve shaker operated for 5 min with an interval operation of 10 s and a shaking amplitude of 1.6 mm. The test results obtained using a total material mass of about 100 g are shown in Fig. 3. In addition, to quantify particle size distributions for different samples, several particle size characteristics are reported in Table 1. Here, D_{10}, D_{50}, and D_{90} represent the particle diameters associated with 10%, 50%, and 90%, respectively, of the total particle mass, e.g., the mass of particles smaller than D_{10} is equal to 10% of the total mass. Moreover, the following parameter

$$\sigma_d = \frac{D_{90} - D_{10}}{D_{50}} \tag{1}$$

represents the span of a particle size distribution.

Furthermore, the Sauter Mean Diameter (SMD), D_{32}, was calculated since it is the most relevant to processes where specific surface area is important for reactivity like dust explosions. In terms of a finite number of discrete size classes, D_{32} is defined as follows:

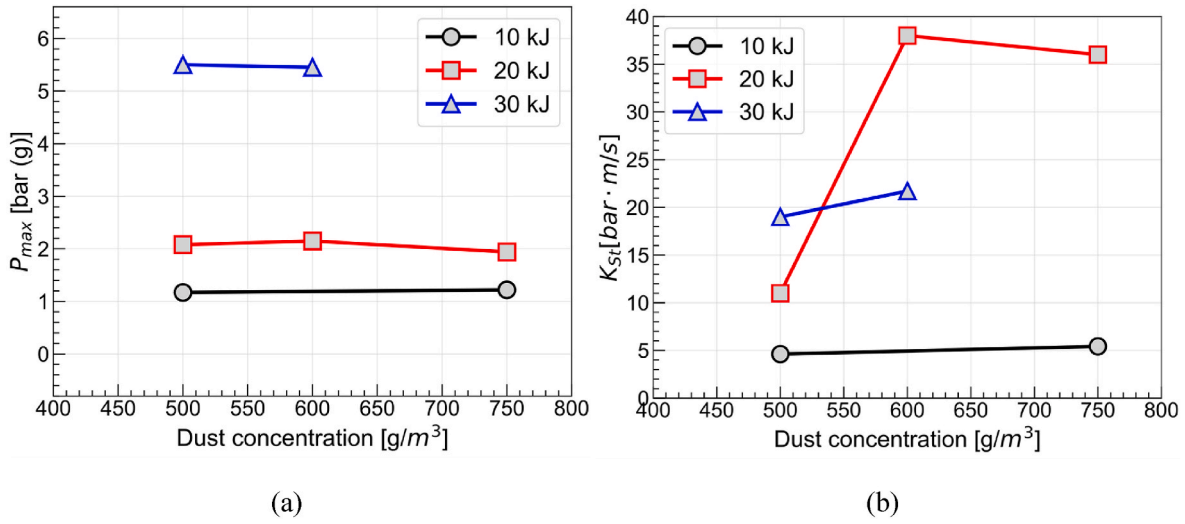

Fig. 7. Maximum explosion overpressure (a) and deflagration index (b) versus concentration of black mass sample D at different ignition energies.

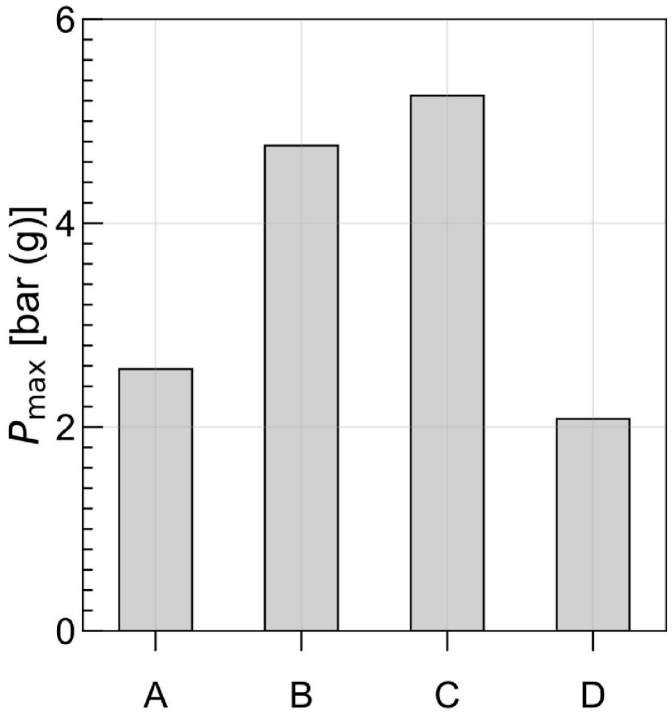

Fig. 8. Maximum explosion overpressures measured for different black mass samples at the dust concentration of 500 g/m^3 and ignition energy of 20 kJ.

$$D_{32} = \frac{\sum_{i=1}^{i=N} n_i D_i^3}{\sum_{i=1}^{i=N} n_i D_i^2}, \quad (2)$$

where n_i is the number of particles in the i-th particle size range; D_i is the mean particle size in the i-th particle size range; N is the total number of particle size ranges. The obtained D_{32} is shown in Table 1.

In addition, Table 1 reports the water content (weight) determined using a Karl-Fischer Titration method with an oven according to ASTM D 6304-07 standard. The samples were titrated with Hydranal Nextgen coulomat A-FA and C-FA as KF reagents from Honeywell. The samples were heated in a Metrohm 832 KF Thermoprep oven at a temperature of 160 °C. A sample mass of 0.5–1.0g was weighed into vials and sealed with a lid. Vapours from the heated sample were transferred to a titrator with dry air and titrated using a coulometry method. The results were calculated from duplicate determinations. The water content is reported based on the whole weight.

2.3. Organic solvents in black mass

Electrolytes used in battery cells consist of organic solvents, such as various carbonates, and salts dissolved in the solvents (Wang et al., 2019). The organic solvents, constituting approximately 10% of the cell mass, may ignite and burn in the presence of the air (Ribière et al., 2012). The organic solvents may also exist in black mass as impurities and may influence the dust explosion characteristics. Therefore, it is necessary to quantify the content of organic carbonates in the black mass.

Two distinct analytical approaches were employed. Initially, the black mass underwent extraction using dichloromethane (DCM) and was subsequently subjected to Gas Chromatograph Mass Spectrometer (GCMS) analysis. The second method utilized Head Space (HS)-GCMS, where the black mass underwent heating within the HS-vial for an hour at 150 °C prior to analyzing the gas content above the material. The results obtained via GCMS are presented here due to its superior quantitative capabilities compared to the HS-GCMS method. Concurrently, HS-GCMS served as a supplementary technique for qualitative analysis, particularly in identifying volatile compounds within the black mass. Among the identified organic carbonates, ethylene carbonate ($C_3H_4O_3$, EC) predominated, with minor traces of other compounds observed; see Table 2. Notably, sample C yielded no detectable carbonates using the current methodologies.

3. Dust explosion experimental setups

The dust explosion experiments were conducted in a 20 L vessel manufactured by Anko, as sketched in Fig. 4. First, a vacuum pressure of −0.6 bar gauge was created by evacuating air from the spherical vessel. Second, the dust sample was loaded into a pressurized container at 20

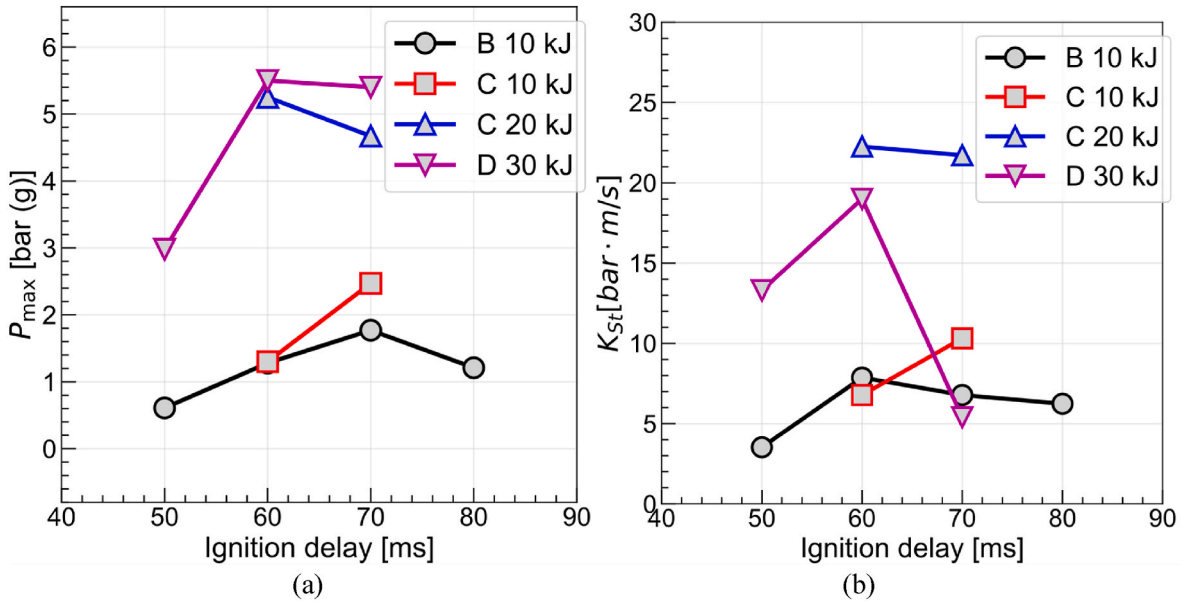

Fig. 9. Effect of ignition delay time on the maximum explosion overpressure (a) and deflagration index (b) for black mass samples B, C and D with various ignition energies.

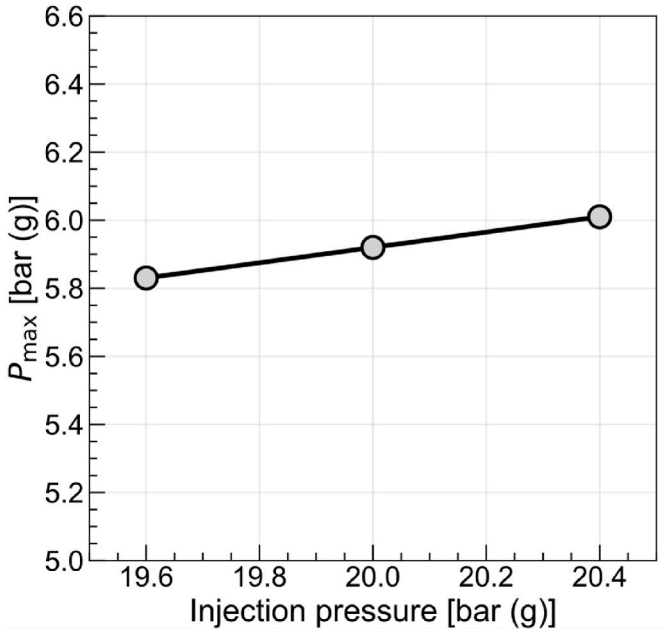

Fig. 10. Maximum explosion overpressures measured for black mass C at the dust concentration of 300 g/m^3 and an ignition energy of 20 kJ.

bar gauge. Third, the dust was injected into the spherical chamber via a fast-actuating valve and a rebound V-shape nozzle. After the dust injection, a relatively homogenous dust-air cloud was formed and the pressure within the vessel stabilized at approximately 1 atm according to the standard, e.g., EN 14034-1. Fourth, pyrotechnical igniters were employed to ignite the dust cloud after a variable ignition delay time, i.e., time interval between the dust injection and ignition. Fifth, the pressure curve $P(t)$ was recorded using dynamic pressure sensors. Finally, the rate of pressure rise was calculated by differentiating $P(t)$.

4. Results and discussions

Different parameters were varied to study black mass dust explosion, as summarized in Table 3. Totally, around 70 experiments were performed in the 20-L vessel.

Fig. 5 shows (a) a typical pressure-curve $P(t)$ and (b) its derivative dP/dt in the case of successful ignition of a dust cloud. The focus of the following discussion will be placed on (a) the maximum explosion overpressure P_{max} and (b) the deflagration index, $K_{St} = (dP/dt)_{max} V^{1/3}$, which is proportional to the maximum pressure growth rate $(dP/dt)_{max}$. These two quantities are show in filled black-grey circles in Fig. 5(a) and (b), respectively.

Black circles in Fig. 6 (a) show that black mass dust explosion experiments with the 10 kJ ignitor have yielded an overpressure around 1 bar for all studied samples, thus, indicating weak explosion process. On the contrary, the 20 kJ ignitor is able to initiate sufficiently intense combustion of black mass, which yields a relatively high explosion overpressure; see red squares in Fig. 6 (a), with dependence of the maximum explosion overpressure on dust concentration being typically of a parabolic shape. However, a further increase in the ignition energy weakly affects P_{max} for sample C, cf. red squares and blue triangles. Dependence of the deflagration index K_{St} on dust concentration also has a parabolic shape when using the 20 kJ ignitor; see Fig. 6 (b). Note that the 20 and 30 kJ ignitors were assembled by combining two and three pairs of 10 kJ (2 × 5 kJ) chemical ignitors, as used in the standard tests. These ignitors were tied on two electrodes with approximately uniform spaces between the ignitors. We avoid directing the ignitors toward the dynamic pressure sensors.

For black mass sample D, an increase in the ignition energy results in increasing P_{max}; see Fig. 7 (a). However, there is no obvious trend in K_{St} regarding the ignition energy; see Fig. 7 (b). Comparison of Figs. 6 and 7 indicates that, at the ignition energy of 20 kJ, explosion risk is significantly higher for sample C than for sample D.

Comparison of maximum explosion overpressures for different samples at a dust concentration of 500 g/m^3 and an ignition energy of 20 kJ is shown in Fig. 8. Samples B and C generate P_{max} higher than 4.5 bar, whereas samples A and D yield a significantly lower P_{max}. More

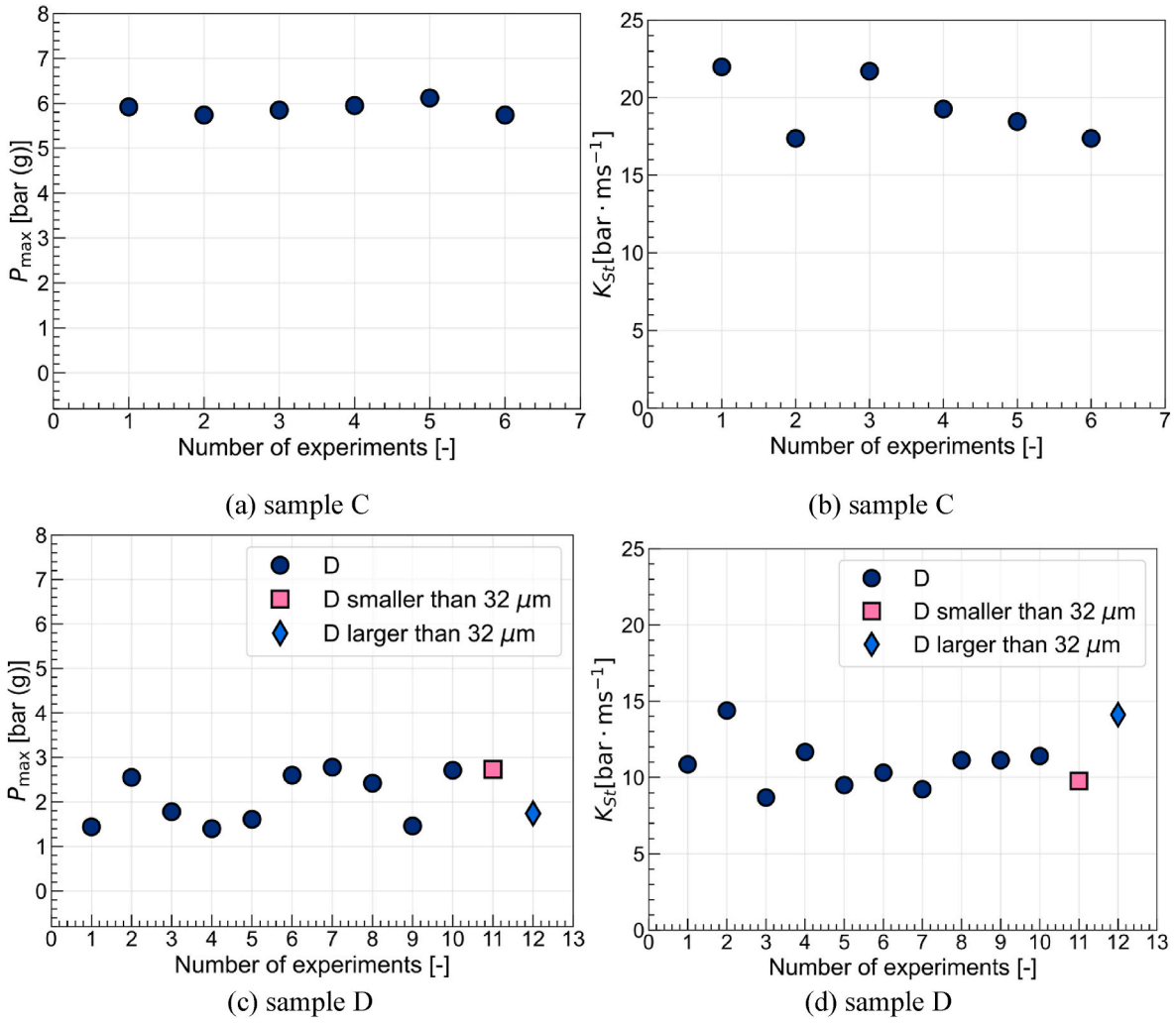

Fig. 11. Repeated dust explosion experiments for dust sample C at a concentration of 300 g/m^3 and D at a concentration of 500 g/m^3 with an ignition energy of 20 kJ.

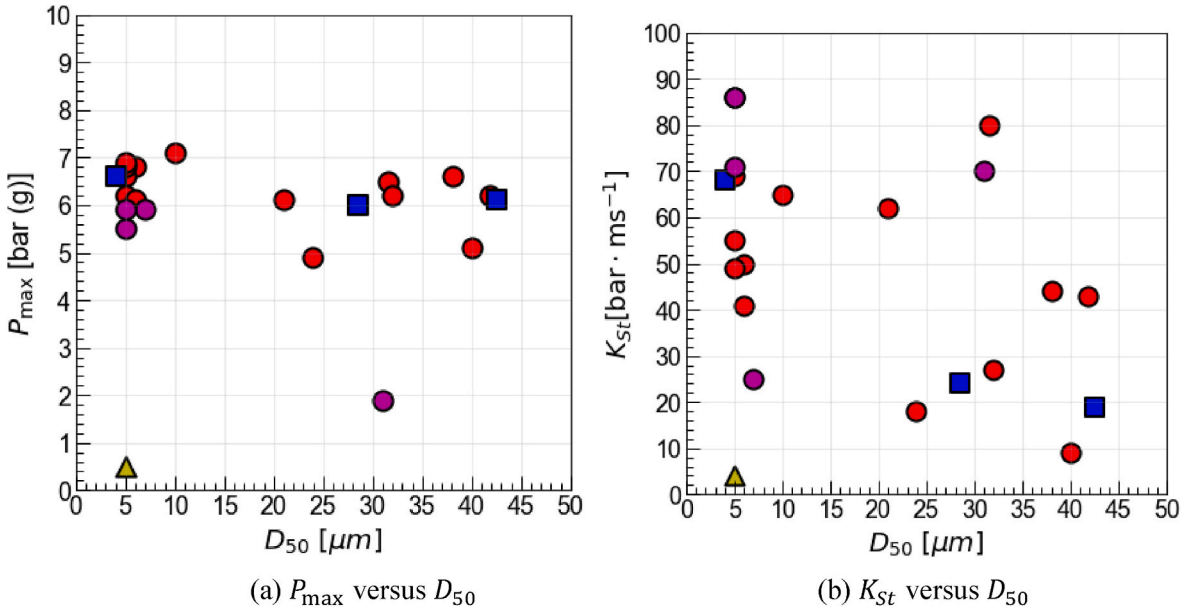

(a) P_{max} versus D_{50} (b) K_{St} versus D_{50}

Fig. 12. Dust explosion characteristics P_{max} and K_{St} versus D_{50} for 35 graphite dust samples from the literature, i.e., red circles (Gestis-Dust-Ex, 2024), magenta circles (Beck et al., 1997), blue squares (Denkevits and Dorofeev, 2005), and yellow triangle (Phylaktou et al., 2015). (For interpretation of the references to colour in this figure legend, the reader is referred to the Web version of this article.)

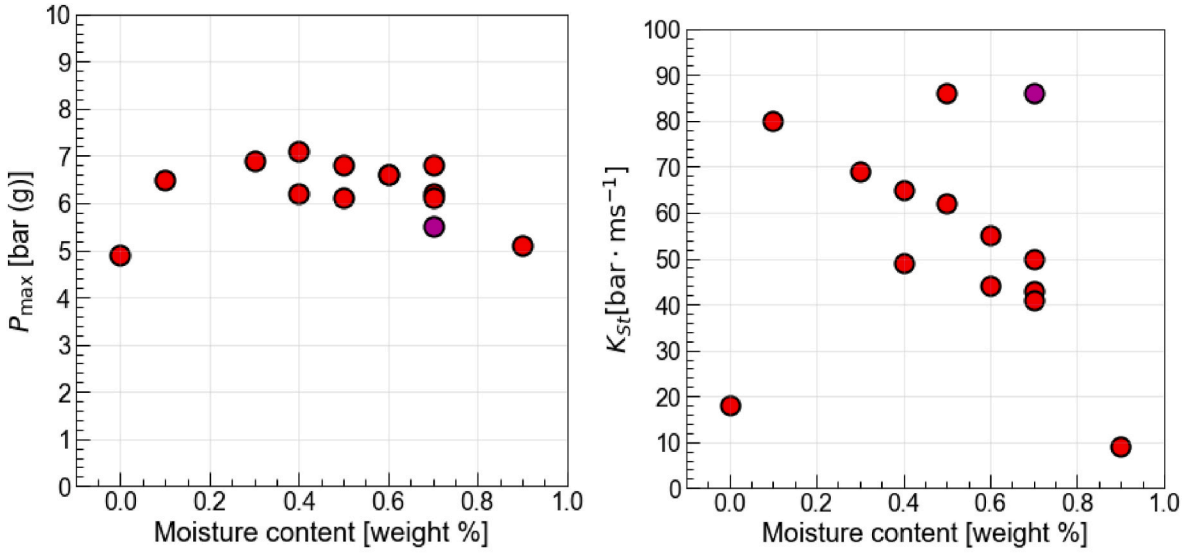

(a) P_{max} versus moisture content (b) K_{St} versus moisture content

Fig. 13. Dust explosion characteristics P_{max} and K_{St} versus moisture content for 35 graphite dust samples from the literature, i.e., red circles (Gestis-Dust-Ex, 2024) and magenta circles (Beck et al., 1997). (For interpretation of the references to colour in this figure legend, the reader is referred to the Web version of this article.)

research is needed to provide detailed explanations for these findings. At a first glance, the differences could be attributed to different water contents; see Table 1, which shows that sample A has a relatively higher water content compared to other samples. Alternatively, the difference could be due to different chemical compositions of the black mass samples, their volatile content or fixed carbon content, because the samples came from different process plants.

Note that the difference between samples A and B mainly lies in the content of organic solvents, according to the black mass supplier. This fact is confirmed by measurements in GCMS; see Table 2. Sample A contains 2.99 % ethylene carbonate, whereas sample B contains only 0.014 %. It is unclear if lower P_{max} generated by sample A is due to the impurities of EC or due to the larger particle size (D_{32} is 38 μm for sample A and 22 μm for sample B). More analyses of the samples' chemical composition are needed. Sample D yields substantially lower P_{max} when compared to sample C at a dust concentration of 500 g/m^3 and an ignition energy of 20 kJ. The reason may lie in the fact of different material compositions, since the two samples were provided by

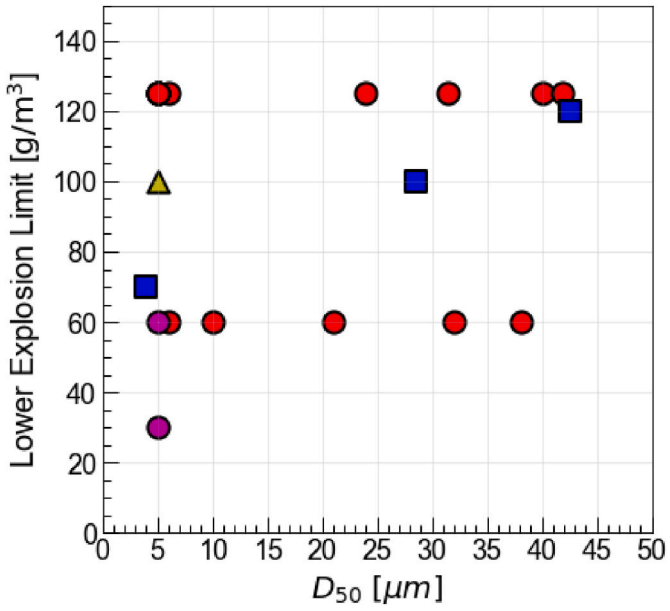

Fig. 14. Lower explosion limit versus D_{50} for 35 graphite dust samples from the literature, i.e., red circles (Gestis-Dust-Ex, 2024), magenta circles (Beck et al., 1997), blue squares (Denkevits and Dorofeev, 2005), and yellow triangle (Phylaktou et al., 2015). (For interpretation of the references to colour in this figure legend, the reader is referred to the Web version of this article.)

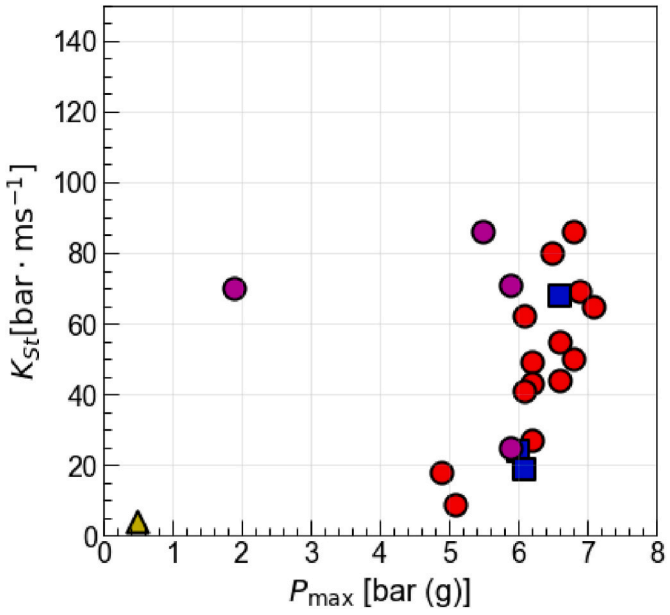

Fig. 15. K_{St} versus P_{max} for 35 graphite dust samples from the literature, i.e., red circles (Gestis-Dust-Ex, 2024), magenta circles (Beck et al., 1997), blue squares (Denkevits and Dorofeev, 2005), and yellow triangle (Phylaktou et al., 2015). (For interpretation of the references to colour in this figure legend, the reader is referred to the Web version of this article.)

two different suppliers. Note that sample C contains a higher content of graphite, as indicated by one supplier. Graphite (main battery anode material) has a higher dust explosion risk compared to metal oxide (main battery cathode material). Furthermore, sample D has a higher content of organic solvent, see Table 2, which could lead to a less uniform distribution of dust air cloud in the vessel at the ignition instance.

The effect of ignition delay time on P_{max} is shown in Fig. 9. The ignition delay time mainly controls the turbulence characteristics in the vessel at the ignition instance. For black mass powders B and C and the ignition energy of 10 kJ, the highest P_{max} (but still low) was measured at ignition delay time of 70 ms, see black circles and red squares in Fig. 9 (a). Note that this delay time is longer than the recommended standard value of 60 ms. However, the standard delay time yields the largest P_{max} in the case of a higher ignition energy and intense dust combustion, see blue and violet triangles, which show results obtained from samples C and D, respectively, using ignition energy of 20 kJ and 30 kJ, respectively. Deflagration index is also largest in these two cases, see Fig. 9 (b).

Maximum explosion overpressures measured using black mass sample C and varying the dust injection pressure are reported in Fig. 10. P_{max} increases linearly with the injection pressure, in line with the results by Spitzer et al. (2022), obtained using cornstarch. but these results are limited to a narrow range of the injection pressure variations allowed by the used equipment.

Finally, Fig. 11 shows the scatter of the measured data from repeated tests for samples C and D. The measured P_{max} fluctuates less for sample C when compared to sample D, with a standard derivation for P_{max} for samples C and D being equal to 0.14 and 0.58, respectively. On the contrary, the measured K_{St} for sample D fluctuates slightly less compared to that for sample C, with a standard derivation for samples D and C being equal to 1.60 and 2.08, respectively. Comparison of different symbols in Fig. 11 (c) or (d) indicates weak influence of particle size on the measured maximum overpressure and deflagration index.

5. Comparison with other dusts

In addition to black mass, many other materials are handled during battery recycling process, such as graphite, aluminium, copper, iron, and plastic, etc. In this report, we focus exclusively on black mass, graphite, and aluminium. The dust explosion characteristics include maximum explosion overpressure (P_{max}), deflagration index (K_{St}), minimum ignition energy, and minimum ignition temperature of dust layer and cloud. The data have been collected from various sources including (i) a report by Beck et al. (1997), (ii) Gestis-Dust-Ex database (2024), (iii) a book by Eckhoff (2003), and (iv) other publications.

5.1. Dust explosion characteristics of graphite

The literature has extensively investigated the impact of particle size on dust explosion characteristics (Cashdollar, 2000; Castellanos et al., 2014; Dufaud et al., 2010; Kuai et al., 2011; Mittal, 2014). Generally, smaller particles, such as those in the micrometre range exhibit higher values of P_{max} and K_{St}, e.g., for coal (Cashdollar, 2000), iron (Castellanos et al., 2014), aluminum (Dufaud et al., 2010; Castellanos et al., 2014), and magnesium (Kuai et al., 2011; Mittal, 2014) dusts. This trend is attributed to the larger specific surface area of smaller particles, which enhances volatilization and burning rates (Castellanos et al., 2014). However, this trend may not continue for nanoparticles (Eckhoff, 2020). There are two physical reasons (Green and Lane, 1957). First, due to strong inter-particle cohesion forces, it is difficult to complete dispersion of bulk powders consisting of nanoparticles. Second, extremely fast particle coagulation or re-agglomeration can occur for nano powders.

The mass median size, D_{50}, is commonly employed to characterize the average size of dust particles. However, the Sauter Mean Diameter (SMD or D_{32}) offers a more suitable measure for quantifying the average size of dust particles (Dufaud et al., 2010; Castellanos et al., 2014). This is because the SMD reflects the volume-to-surface area ratio which is related to the combustion process during dust explosions. However, such data are often missing in the literature.

Fig. 12 shows P_{max} and K_{St} versus D_{50} for graphite dust from different sources. In contrast to the findings in the individual studies (Cashdollar, 2000; Castellanos et al., 2014; Dufaud et al., 2010; Kuai et al., 2011; Mittal, 2014), no clear trend is observed for the collected data. Fig. 13 shows P_{max} and K_{St} versus D_{50} for graphite dust. There is a slight decrease in P_{max} with an increase in moisture content; see Fig. 13 (a),

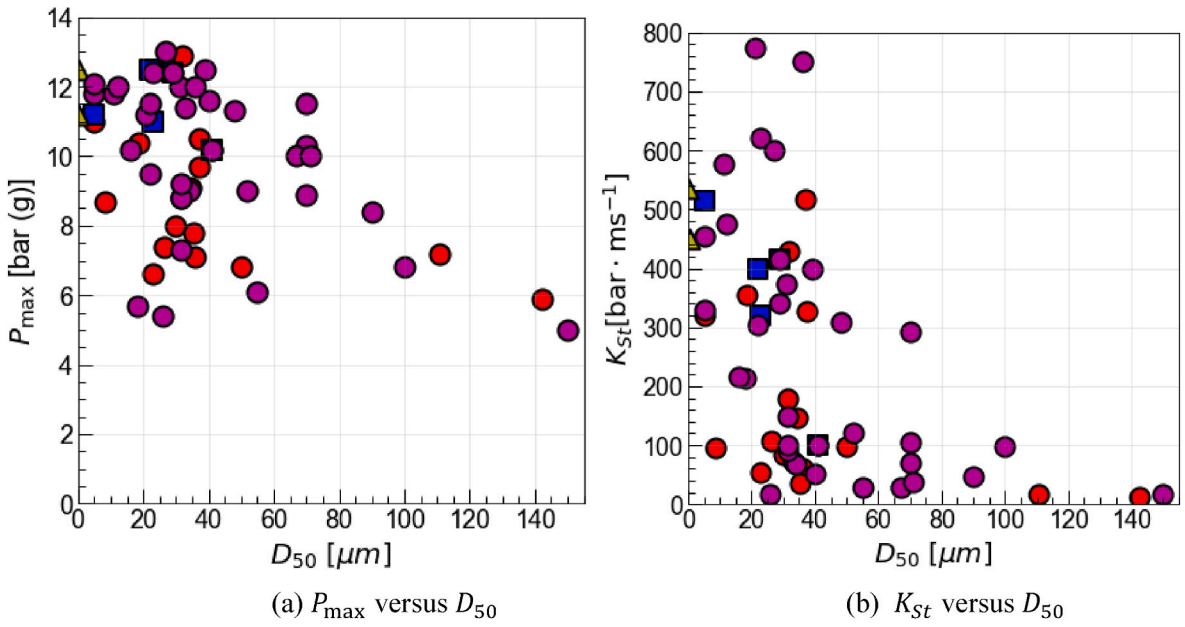

Fig. 16. Dust explosion characteristics P_{max} and K_{St} versus D_{50} for aluminium dust samples from the literature, i.e., red circles (Gestis-Dust-Ex, 2024), magenta circles (Beck et al., 1997), blue squares in Ref. (Eckhoff, 2003), and yellow triangle (Holbrow et al., 2010). (For interpretation of the references to colour in this figure legend, the reader is referred to the Web version of this article.)

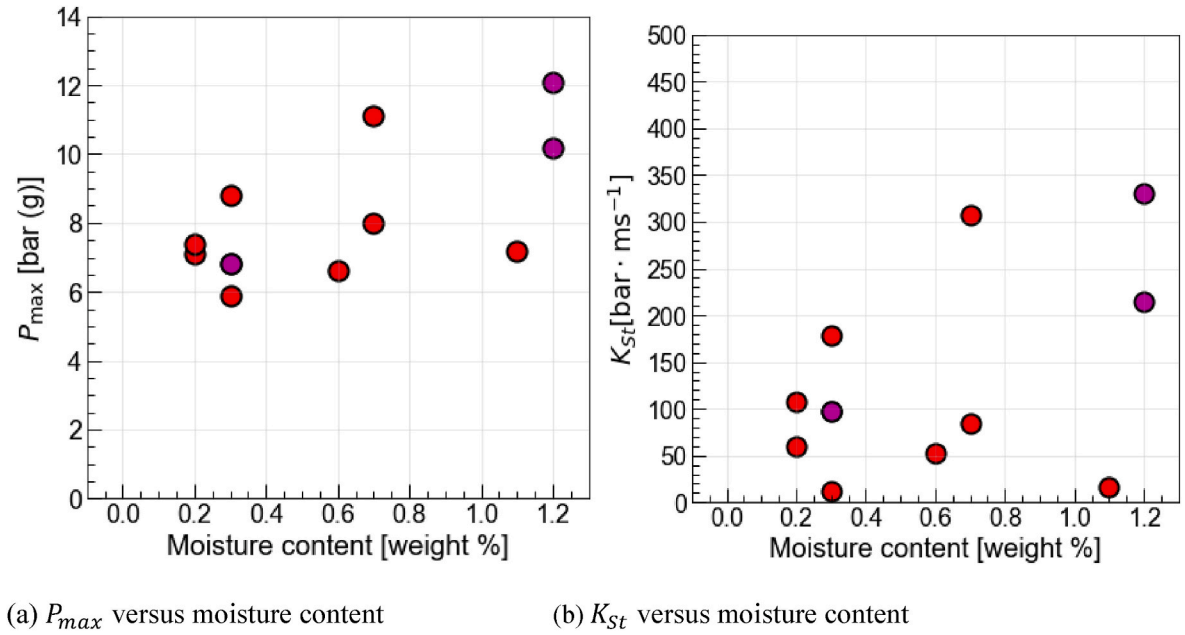

Fig. 17. Dust explosion characteristics P_{max} and K_{St} versus moisture content for aluminium dust samples from the literature, i.e., red circles (Gestis-Dust-Ex, 2024) and magenta circles (Beck et al., 1997). (For interpretation of the references to colour in this figure legend, the reader is referred to the Web version of this article.)

and this trend is more pronounced for K_{St}; see Fig. 13 (b). Notably, the dust explosion characteristics in report by Beck et al. (1997) covers around 4300 dust samples. The online database Gestis-Dust-Ex (2024) contains around 7000 dust sample results, of which 4300 samples are from the report by Beck et al. (1997). Also worth noting is that the moisture content was determined by carefully drying the dust until a constant weight is achieved (Beck et al., 1997). Accordingly, not only water but also some lower boiling point chemicals might be evaporated.

Fig. 14 shows lower explosion limit (LEL) versus D_{50} for graphite dust. Only the data by Denkevits and Dorofeev (2005) show a clear trend of decreasing LEL with decreasing D_{50}; see blue squares in Fig. 14. The rest of the data does not show any trend. The reason may be due to unquantified impurities of graphite dust from different processes in the Gestis-Dust-Ex database. For instance, one graphite dust came "from exhaust system", whereas another graphite dust came "from precipitator" during milling. K_{St} increases with an increase in P_{max} for graphite dust; see Fig. 15.

5.2. Dust explosion characteristics of aluminium

A total number of 107 aluminium dust explosion data were collected. In line with the literature (Cashdollar, 2000; Castellanos et al., 2014; Kuai et al., 2011; Mittal, 2014; Dufaud et al., 2010), P_{max} and K_{St} decrease with an increase in D_{50} for aluminium dust; see Fig. 16. In

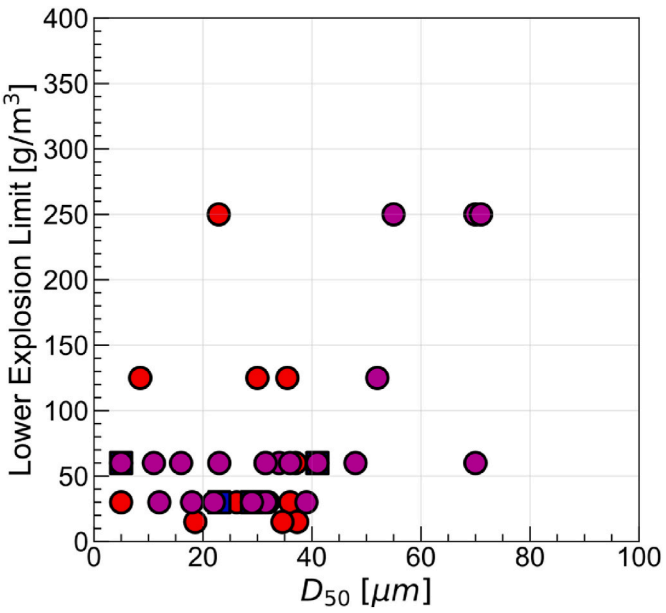

Fig. 18. Lower explosion limit versus D_{50} for aluminium dust samples from the literature, i.e., red circles (Gestis-Dust-Ex, 2024), magenta circles (Beck et al., 1997), blue squares in Ref. (Eckhoff, 2003), and yellow triangle (Holbrow et al., 2010). (For interpretation of the references to colour in this figure legend, the reader is referred to the Web version of this article.)

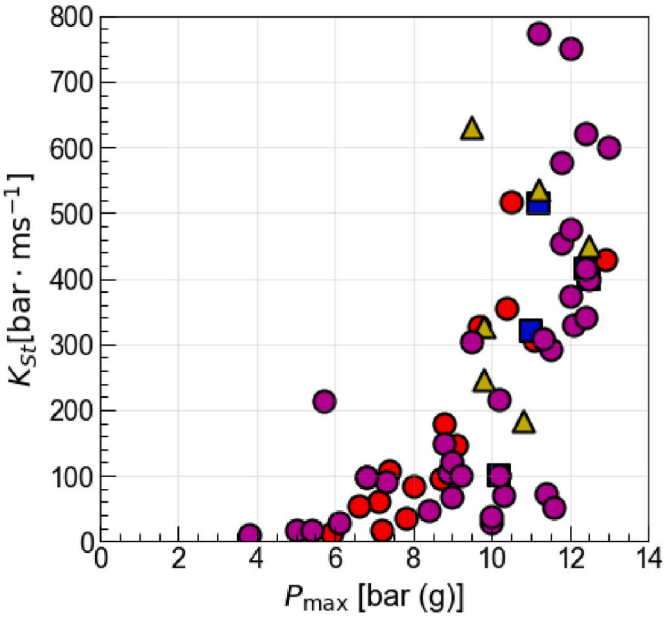

Fig. 19. K_{St} versus P_{max} for aluminium dust samples from the literature, i.e., red circles (Gestis-Dust-Ex, 2024), magenta circles (Beck et al., 1997), blue squares in Ref. (Eckhoff, 2003), and yellow triangle (Holbrow et al., 2010). (For interpretation of the references to colour in this figure legend, the reader is referred to the Web version of this article.)

contrast to the graphite dust, $P_{\max}$ and K_{St} increase with an increase in moisture content for aluminium dust; see Fig. 17. This may be attributed to the fact that aluminium reacts with water and releases hydrogen which accelerates the aluminium dust explosion process. No obvious trend is observed for LEL and D_{50}; see Fig. 18. K_{St} increases with increase of $P_{\max}$ for aluminium dust; see Fig. 19.

5.3. Maximum explosion overpressure and deflagration index

Comparison among black mass, graphite, and aluminium dust explosion parameters is shown in Fig. 20. Note that $P_{\max}$ and K_{St} are average values of 35 graphite dust samples and 107 aluminium dust samples. For black mass dusts, a relatively low ignition energy, i.e., 10 kJ, generates mild explosions, which means low values of $P_{\max}$ and K_{St}; see dark blue circles in Fig. 20. However, a relatively high ignition energy, i.e., 20 kJ, generates high explosion overpressures, around 6 bar for black mass sample C; see Fig. 20 (a). Aluminium dust is the most hazardous dust among the three, with an average $P_{\max}$ being 9. 8 bar and an average K_{St} being 263 bar ms^{-1}. Note the logarithmic scale of the ordinate axis in Fig. 20 (b).

5.4. Minimum ignition energy

Comparison of minimum ignition energies among black mass, graphite, and aluminium dusts are shown in Fig. 21. Again, aluminium dust requires the lowest ignition energy, as low as 1 mJ for some dust samples, followed by graphite dust with the lowest MIE being around 1 J. Black mass dust samples require high MIE, around 10 kJ for samples B, and C, and even larger energy like 20 kJ for samples A and D. In Fig. 21, an ignition is defined as $P_{\max} \geq P_{ign} + 0.5$ bar, according to EN 14034 -3 standard, where P_{ign} is the overpressure produced by the ignitor.

Such a large ignition energy, i.e., more than 10 kJ, occurs seldom in industrial settings. For instance, maximum theoretical spark energies from discharge of various types of electrically conducting objects like screw, 100 mm flange, shovel, large container, and road tanker, lie within 0.05–450 mJ (Glor, 1988). Electrostatic discharges in various forms such as corona, brush, spark, and propagating brush, have an approximate maximum energy around 100 J (Glor, 1988). However, much larger ignition energies may be released during hot works like welding or fires. For instance, a prismatic 1880 mAh LIB cell at 100 % state of charge (SOC) releases 113 ± 19 kJ heat as a result of combustion of the ejected battery materials, i.e., flammable gas, liquids and particles during failure (Said et al., 2019).

It is worth noting that the minimum ignition energies for graphite and aluminium, reported above, were obtained from the literature (Beck et al., 1997; Gestis-Dust-Ex, 2024). In those tests, the dust samples were ignited by a continuous spark generated by a high voltage transformer between two electrodes in the modified Hartmann tube following the standards, e.g., EN ISO/IEC 80079-20. In the present tests performed with the black mass samples, no propagating flames were observed in the modified Hartmann apparatus in the screening test. Therefore, the MIEs for the black mass samples were obtained in the 20-L apparatus using the chemical ignitors.

5.5. Minimum ignition temperature of dust layer and cloud

In general, dust cloud requires higher Minium Ignition Temperature (MIT) when compared to dust layer for both graphite and aluminium dusts; see Fig. 22. Furthermore, aluminium dust requires lower MIT than graphite dust both for dust layer and for dust cloud; see Fig. 22.

6. Conclusions

Four black mass samples from different battery recycling plants were analyzed to obtain dust sample microscope images, particle size distributions, water contents and organic solvent contents. Subsequently, dust explosion experiments were performed in a 20-L vessel by varying the dust concentration, ignition energy, ignition delay, and dust injection pressure. Results show that an ignition energy of 10 kJ is not sufficient to generate a high explosion overpressure, whereas an ignition energy of 20 kJ can yield an explosion overpressure above 6 bar for black mass sample C at a concentration of 300 $\mathrm{g/m}^3$. So high ignition energy could be released during hot works like welding, fire, gas

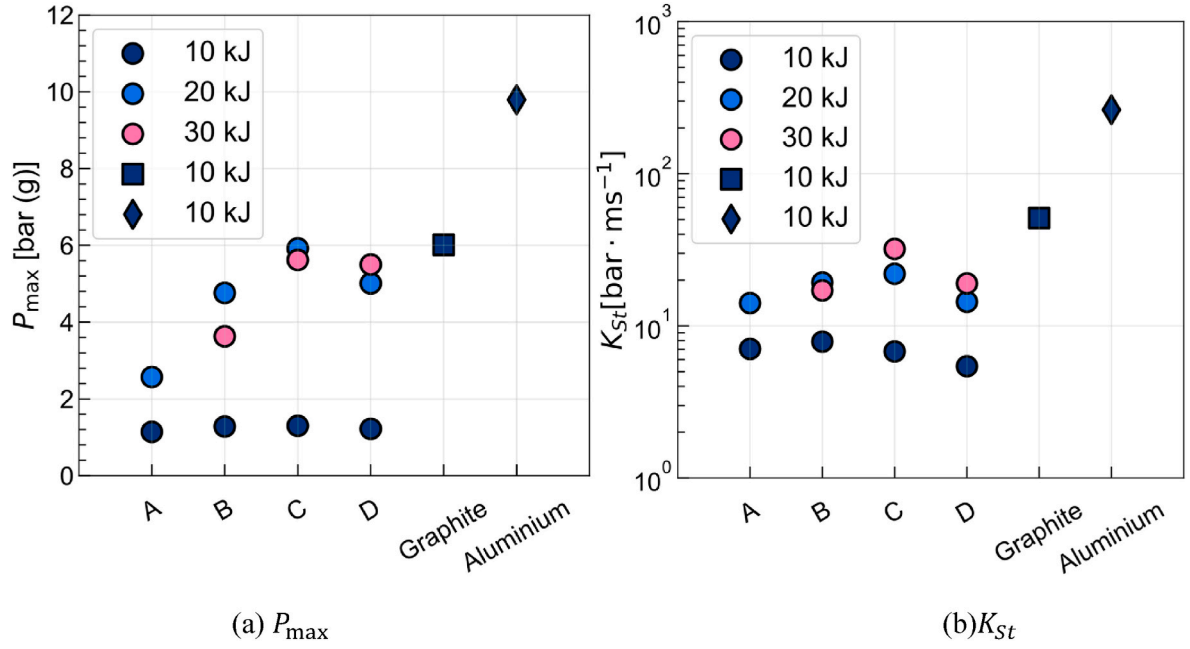

Fig. 20. Comparison of dust explosion characteristics P_{max} and K_{St} among four types of black mass, A, B, C, D, graphite (Gestis-Dust-Ex, 2024; Beck et al., 1997; Denkevits and Dorofeev, 2005; Phylaktou et al., 2015), and aluminium (Gestis-Dust-Ex, 2024; Beck et al., 1997; Eckhoff, 2003; Holbrow et al., 2010). Dark blue circles represent ignition energy of 10 kJ; light blue circles represent ignition energy of 20 kJ; pink circles represent ignition energy of 30 kJ. (For interpretation of the references to colour in this figure legend, the reader is referred to the Web version of this article.)

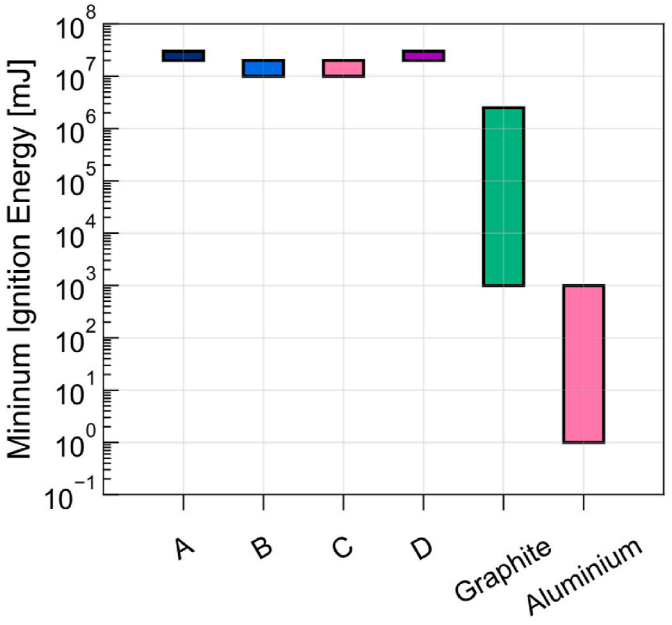

Fig. 21. Comparison of Minium Ignition Energies among four types of black mass, A, B, C, D, graphite (Beck et al., 1997; Gestis-Dust-Ex, 2024), and aluminium (Beck et al., 1997; Gestis-Dust-Ex, 2024).

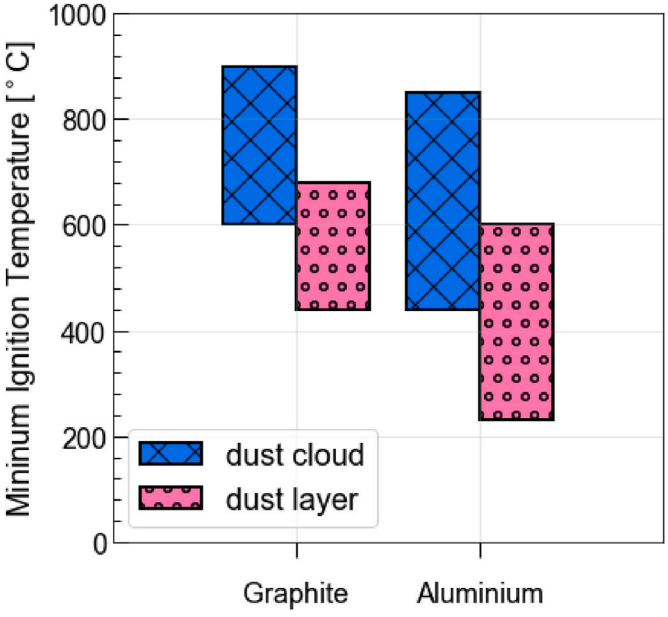

Fig. 22. Comparison of Minium Ignition Temperatures of dust layer and dust cloud for graphite (Beck et al., 1997; Gestis-Dust-Ex, 2024) and aluminium (Beck et al., 1997; Eckhoff, 2003; Gestis-Dust-Ex, 2024) dusts.

explosion due to smouldering or battery failure. Comparison of dust explosion characteristics measured for black mass samples in this study with the counterpart characteristics for graphite and aluminium dusts, taken from the literature was carried out. The aluminium dust generates the highest explosion overpressure and deflagration index among these dusts, indicating the highest risks in the battery recycling plants.

CRediT authorship contribution statement

Chen Huang: Writing – review & editing, Writing – original draft, Project administration, Methodology, Funding acquisition, Conceptualization. **Andrei N. Lipatnikov:** Writing – review & editing, Writing – original draft, Methodology, Conceptualization. **Cecilia Lövström:** Investigation, Visualization. **Nijaz Smajovic:** Investigation. **Leena Andersson:** Investigation. **Abdelrahman Ismail:** Investigation, Writing – original draft.

Declaration of competing interest

The authors declare that they have no known competing financial interests or personal relationships that could have appeared to influence the work reported in this paper.

Acknowledgements

The Swedish Energy Agency is greatly acknowledged through Safe-Dust ReLIB project (number P2023-00060), a pre-study on dust explosion risks for Lithium-Ion Battery Recycling. The authors would like to acknowledge the support of Northvolt Revolt AB and Stena Recycling International AB for providing samples and for valuable discussions. Nathália Vieceli, Zari Musavi, Björn Hall, and Mengqiao Di are greatly acknowledged. Michael Magnusson and Sven-Gunnar Gustafsson are acknowledged for their support in performing risk analysis for dust explosion experiments. Patrik Nilsson, Peter Lindqvist are acknowledged for their measurements of dust explosions in 20-L vessel.

Data availability

Data will be made available on request.

References

Ali, H., Khan, H.A., Pecht, M., 2022. Preprocessing of spent lithium-ion batteries for recycling: need, methods, and trends. Renew. Sustain. Energy Rev. 168, 112809. https://doi.org/10.1016/j.rser.2022.112809.

Anko, 2017. 20-liter Sphere Apparatus for Determination of Explosive Characteristics of Dust Clouds.

Argus, 2021. Explosion hits CATL battery precursors plant in China. https://www.argusmedia.com/en/news-and-insights/latest-market-news/2175179-explosion-hits-catl-battery-precursors-plant-in-china. (Accessed 28 May 2024).

Beck, H., Glienke, N., Möhlmann, C., 1997. Combustion and explosion characteristics of dusts. HVBG. Federation of the Statutory Accident Lnsurance Lnstitutions of the Lndustrial Sector. https://www.dguv.de/medien/ifa/en/pub/rep/pdf/rep02/biar1397/report-13-97.pdf. (Accessed 28 May 2024).

Cashdollar, K.L., 2000. Overview of dust explosibility characteristics. J. Loss Prev. Process. Ind. 13 (3–5), 183–199. https://doi.org/10.1016/S0950-4230(99)00039-X.

Castellanos, D., Carreto-Vazquez, V.H., Mashuga, C.V., et al., 2014. The effect of particle size polydispersity on the explosibility characteristics of aluminum dust. Powder Technol. 254, 331–337. https://doi.org/10.1016/j.powtec.2013.11.028.

CRM list, 2023. Critical, strategic and advanced materials. https://rmis.jrc.ec.europa.eu/eu-critical-raw-materials. (Accessed 28 May 2024).

Denkevits, A., Dorofeev, S., 2005. Dust explosion hazard in ITER: explosion indices of fine graphite and tungsten dusts and their mixtures. Fusion Eng. Des. 75–79, 1135–1139. https://doi.org/10.1016/j.fusengdes.2005.06.032.

Directive 2000/53/EC, 2000. Directive 2000/53/EC of the European parliament and of the council of 18 september 2000 on end-of life vehicles. http://data.europa.eu/eli/dir/2000/53/oj. (Accessed 28 May 2024).

Directive 2012/19/EU, 2012. Directive 2012/19/EU of the European Parliament and of the Council of 4 July 2012 on waste electrical and electronic equipment (WEEE). https://eur-lex.europa.eu/legal-content/sv/TXT/?uri=CELEX:32012L0019#d1e32-53-1. (Accessed 28 May 2024).

Dufaud, O., Traoré, M., Perrin, L., et al., 2010. Experimental investigation and modelling of aluminum dusts explosions in the 20 L sphere. J. Loss Prev. Process. Ind. 23 (2), 226–236. https://doi.org/10.1016/j.jlp.2009.07.019.

Eckhoff, R.K., 2003. Dust Explosions in the Process Industries, third ed. Elsevier.

Eckhoff, R.K., 2020. Fighting dust explosion hazards in the process industries. J. Loss Prev. Process. Ind. 67, 104225. https://doi.org/10.1016/j.jlp.2020.104225.

Elektrikern, 2024. En dammexplosion i veckan kan drabba elektriker – ändå missar företagen risken. https://tidningenelektrikern.se/2024/04/29/en-dammexplosion-i-veckan-anda-missar-foretagen-risken/. (Accessed 28 May 2024).

Gestis-Dust-Ex, 2024. Database Combustion and explosion characteristics of dusts. https://www.dguv.de/ifa/gestis/gestis-staub-ex/index-2.jsp. (Accessed 28 May 2024).

Glor, M., 1988. Electrostatic Hazards in Power Handling.

Green, H.L., Lane, W.E., 1957. Particulate Clouds: Dusts, Smokes and Mists. Their Physios and Physical Chemistry and Industrial and Environmental Aspects. E. & F. N. Spon, Ltd., London.

Harper, G., Sommerville, R., Kendrick, E., et al., 2019. Recycling lithium-ion batteries from electric vehicles. Nat 575, 75–86. https://doi.org/10.1038/s41586-019-1682-5.

Independent, 2021. Explosion at Chinese battery recycling plant kills one and injures 20. https://www.independent.co.uk/news/world/asia/explosion-blast-china-battery-fire-hunan-b1784643.html. (Accessed 28 May 2024).

Kim, S., Bang, J., Yoo, J., et al., 2021. A comprehensive review on the pretreatment process in lithium-ion battery recycling. J. Clean. Prod. 294, 126329. https://doi.org/10.1016/j.jclepro.2021.126329.

Kuai, N., Li, J., Chen, Z., et al., 2011. Experiment-based investigations of magnesium dust explosion characteristics. J. Loss Prev. Process. Ind. 24 (4), 302–313. https://doi.org/10.1016/j.jlp.2011.01.006.

Mittal, M., 2014. Explosion characteristics of micron- and nano-size magnesium powders. J. Loss Prev. Process. Ind. 27, 55–64. https://doi.org/10.1016/j.jlp.2013.11.001.

Navarro, R.P., Seidel, P., Lenz, L., et al., 2022. European battery recycling: an emerging cross-industry convergence. https://www.adlittle.com/sites/default/files/viewpoints/ADL_European_battery_recycling.pdf. (Accessed 28 May 2024).

Phylaktou, H.N., Andrews, G.E., Mkpadi, M., et al., 2015. The explosibility of graphite powder; the effects of ignition energy, graphite concentration and graphite age. In: 16th International Nuclear Graphite Specialists Meeting, pp. 13–17.

Regulation (EU) 2023/1542, 2023. Regulation (EU) 2023/1542 of the European parliament and of the council of 12 July 2023 concerning batteries and waste batteries, amending directive 2008/98/EC and regulation (EU) 2019/1020 and repealing directive 2006/66/EC. https://eur-lex.europa.eu/eli/reg/2023/1542/oj. (Accessed 28 May 2024).

Regulation (EU) 2024/1252, 2024. Regulation (EU) 2024/1252 of the European Parliament and of the Council of 11 April 2024 establishing a framework for ensuring a secure and sustainable supply of critical raw materials and amending Regulations (EU) No 168/2013, (EU) 2018/858, (EU) 2018/1724 and (EU) 2019/1020Text with EEA relevance. http://data.europa.eu/eli/reg/2024/1252/oj. (Accessed 28 May 2024).

Ribière, P., Grugeon, S., Morcrette, M., et al., 2012. Investigation on the fire-induced hazards of Li-ion battery cells by fire calorimetry. Energy Environ. Sci. 5 (1), 5271–5280. https://doi.org/10.1039/C1EE02218K.

Said, A.O., Lee, C., Liu, X., Wu, Z., Stoliarov, S.I., 2019. Simultaneous measurement of multiple thermal hazards associated with a failure of prismatic lithium ion battery. Proc. Combust. Inst. 37 (3), 4173–4180. https://doi.org/10.1016/j.proci.2018.05.066.

Sattar, A., Cooper, L., Dowson, M., et al., 2022. Health and Safety Considerations in Lithium-Ion Battery Recycling.

Spitzer, S.H., Askar, E., Benke, A., Janovsky, B., Krause, U., Krietsch, A., 2022. Influence of pre-ignition pressure rise on safety characteristics of dusts and hybrid mixtures. Fuel 311, 122495. https://doi.org/10.1016/j.fuel.2021.122495.

SVT Nyheter, 2023a. Explosion i Northvolts batterifabrik i Skellefteå – en person brännskadad. https://www.svt.se/nyheter/lokalt/vasterbotten/explosion-pa-northvolt-en-skadad–uffx0g. (Accessed 28 May 2024).

SVT Nyheter, 2023b. https://www.svt.se/nyheter/lokalt/vasterbotten/25-aring-som-skadades-i-explosion-pa-batterifabriken-har-avlidit–llrqtv. (Accessed 28 May 2024).

Wang, Q., Mao, B., Stoliarov, S.I., et al., 2019. A review of lithium ion battery failure mechanisms and fire prevention strategies. Prog. Energy Combust. Sci. 73, 95–131. https://doi.org/10.1016/j.pecs.2019.03.002.

Yi, C., Zhou, L., Wu, X., et al., 2021. Technology for recycling and regenerating graphite from spent lithium-ion batteries. Chin. J. Chem. Eng. 39, 37–50. https://doi.org/10.1016/j.cjche.2021.09.014.

Yu, D., Huang, Z., Makuza, B., et al., 2021. Pretreatment options for the recycling of spent lithium-ion batteries: a comprehensive review. Miner. Eng. 173, 107218. https://doi.org/10.1016/j.mineng.2021.107218.

Yuan, Z., Khakzad, N., Khan, F., Amyotte, P., 2015. Dust explosions: a threat to the process industries. Process Saf. Environ. Protect. 98, 57–71. https://doi.org/10.1016/j.psep.2015.06.008.